CHARACTERIZATION OF FLASHING JET AEROSOLS WITH A PHASE-DOPPLER ANEMOMETER

Document No.: CW-126520-CONF-001

S.C. Sutradhar

Reactor Safety Division
Atomic Energy of Canada Ltd.
Chalk River Laboratories
Chalk River, Ontario, K0J 1J0.

ABSTRACT

A phase-Doppler anemometer (PDA) was used successfully to measure aerosol size distribution and velocity in high-pressure, high-temperature flashing jets discharging from a nozzle simulating a hypothetical break in the reactor heat-transport system. The basic operating principles of the PDA and the thermodynamics of flashing jets are discussed. The measurements indicate that the velocity decreased, and the smaller aerosols prevailed, as the jet diverged away from the break. The larger aerosols had the tendency to settle below the lower half of the jet axis due to gravitational agglomeration and settling. Higher operating pressures upstream of the break produced higher jet velocity as well as larger aerosols.

1. INTRODUCTION

When a subcooled liquid at high-pressure is discharged through a small break in a pipe or in a container into an atmosphere below the saturation pressure (corresponding to the liquid temperature), the liquid starts boiling spontaneously. Tiny vapour or bubbles in the liquid seemingly ‘explode’, and the explosion shatters the remaining liquid that results in a two-phase discharge from the break. This process of violent explosion and formation of two-phase discharge is termed as ‘flashing jet’. The shattered liquid usually fragments further due to aerodynamic forces, and finally atomizes into a mist of fine aerosol droplets.

Atomization of high-enthalpy coolant is expected in a hypothetical loss-of-coolant accident (LOCA) involving a break in the primary heat-transport system (PHTS) of a CANDU®[1] reactor. During a LOCA, a jet of high-pressure, high-temperature coolant discharges from the break. The jet finally atomizes into a mist of steam (water-droplet aerosols and water vapor) that tends to spread to the large free volume due to air circulation and turbulence inside the containment building. The relatively cool atmosphere inside the building condenses the vapor into more water-droplet aerosols. These aerosols could be the carriers of dissolved fission products or radionuclides (from fuel) [1] and may remain suspended in the containment air for extended periods of time.

These suspended aerosols are subject to phenomena like gravitational agglomeration, settling, diffusiophoresis, thermophoresis, etc., inside the containment building. In the worst-case scenario of a

[1] CANDU® (CANada Deuterium Uranium): a registered trademark of Atomic Energy of Canada Ltd.

prolonged discharge from the break, the containment building pressure can increase and force the aerosols carrying fission products to leak through various leak paths of the building. If the mist of tiny water droplets remains suspended for an extended period of time, a significant quantity of fission products can potentially leak out of containment. On the other hand, if the size of the aerosols is large, more aerosols will tend to deposit inside the containment due to agglomeration and settling, and some may even get trapped inside the containment leak paths.

Physical phenomena of a flashing jet are very complex. Depending on the upstream conditions at the break, a flashing jet can have different discharge rates, and water droplets formed by the jet can have different size distributions. The study of water-droplet aerosols is therefore very important for the assessment of post-accident containment, and to specify the exclusion-area boundary surrounding a nuclear power station if fission-product leakage from containment is deemed a possibility. The SMART-IST code [2] is used for analyzing fission-product transport within containment and out of containment to the atmosphere. The accuracy of SMART calculations depends on the reliable input for the thermalhydraulic boundary conditions of a flashing jet, its discharge rate, and the initial size distribution of aerosols generated at the break inside the post-accident containment.

A phase-Doppler anemometer (PDA) is an excellent device for evaluating various characteristics of aerosols and other microscopic particles embedded in a flow. A PDA is a non-intrusive optical device that can provide simultaneous information on velocity and particle size in high-speed flows. The paper describes the basic principles of a PDA and its successful application to measure aerosol size distribution and velocity in flashing jets discharged from a nozzle representing a break in the reactor heat-transport system.

2. CHARACTERISTICS OF FLASHING JETS

2.1 Jet Formation

The thermodynamic conditions (pressure and temperature) of the liquid upstream of a break (i.e., the stagnation or initial conditions) determine the formation and character of a flashing jet. A high-pressure, high-temperature coolant upstream of the break point is necessary for the formation of a two-phase flashing jet during a LOCA in the reactor heat-transport system. Initially, the coolant resides above the liquid/vapour phase-change line, and once a break occurs, the coolant is released into a lower pressure atmosphere. An important parameter in the study of flashing jets is the 'degree of superheat', ΔT_{sh}, which is the temperature difference between the stagnation condition and the saturation temperature (T_{sat}) corresponding to the pressure (P_{fin}) at the final (or released) condition, i.e., $\Delta T_{sh} = T_{st} - T_{sat}(P_{fin})$. In case the liquid is discharged into the standard atmosphere, the degree of superheat is simply the difference in the stagnation temperature and the standard or ambient boiling temperature ($\Delta T_{sh} = T_{st} - T_{amb}$).

Figure 1 is the schematic representation of a flashing jet on the pressure/enthalpy diagram. Consider the S – P process in Figure 1 where the liquid initially is above the liquid/vapour saturation line, and the liquid pressure decreases rapidly as it exits a break. If the liquid remains subcooled (or above the saturation line) at the exit, then the liquid would emerge from the break as a single-phase jet. Further away from the break, it will disintegrate via aerodynamic interactions and wave instabilities. This type of flashing is common to automotive industry for direct injection engines [3].

The T– P process in Figure 1 shows that the final exit conditions lie below the liquid/vapour saturation line. As the pressure drops below the liquid/vapour saturation line ($\Delta T_{sh} > 0$), then the thermodynamic conditions at the break reach 'superheated' (or saturated two phase) conditions. The so-called 'flashing' process now commences with rapid bubble production and shattering of the liquid during its exit from the break, thus forming aerosols.

2.2 Jet Break-Up

Once a jet exits from a break, it tends to disintegrate or break-up into water-droplet aerosols. Two different mechanisms operate independently in the breaking up of a jet, and they are: (1) mechanical break-up and (2) thermal break-up. The mechanical break-up is independent of the thermodynamic state of the liquid, whereas the thermodynamic state predominates in the thermal break-up. For the mechanical break-up, a jet should flow at sufficiently high speed that results in surface stresses causing liquid droplets of a certain size to become unstable and break-up into smaller droplets. The mean droplet size is a function of jet velocity and nozzle or orifice size [4].

For the thermal break-up, a liquid undergoes a rapid depressurization, but maintains its initial temperature because of thermal inertia (a situation of thermodynamic non-equilibrium), and hence, this temperature remains higher than the saturation temperature corresponding to the pressure at the released environment. The meta-stable liquid returns violently to its equilibrium state through rapid boiling and bubble growth, thus shattering the surrounding liquid into small droplets or aerosols.

The size (or more precisely the mass) of droplets formed by atomization of a jet is an important parameter that determines the severity of subsequent processes inside the reactor containment. Droplet characteristics are often described by a size distribution, from which the mass of liquid discharged can be obtained. Brown and York [4] first proposed droplet size correlations for superheated jets of water and Freon. They found that the distributions were log normal (logarithm of a variable having the normal distribution), and since then, most aerosol studies showed similar size distributions.

3. PHASE-DOPPLER ANEMOMETER

The jet characteristics (droplet size and velocity distribution) were measured using a state-of-the-art phase-Doppler anemometer at the Atomic Energy of Canada Ltd. (AECL). The PDA is an extended version of laser-Doppler anemometer (LDA) that is used extensively for non-intrusive velocity measurement in single- or two-phase flows. The optical arrangements for both PDA and LDA are similar, but PDA utilizes multiple optical receiving units (photomultipliers) for simultaneous measurements of velocity and size distributions. The PDA can also provide data for concentration and mass flux of particles of known density [5 – 7]. Figure 2 shows the schematic of the PDA optical arrangement.

The working principle of the PDA involves splitting coherent light from a laser into two equal beams and focusing them by lens to form a measuring volume that is ellipsoidal in shape with the long axis pointing in the direction of the bisector of the two beams. The short axis of the ellipsoid is primarily dependent on the beam diameter, and varies weakly with beam intersection angle; however, the long axis increases rapidly with decreasing beam angle. Typical measuring volume dimensions are 0.1 mm in diameter and 1-mm long. When the two laser beams cross, they interfere to form a set of fringes at the plane of beam crossing (on the x-z plane in Figure 2), and the fringe spacing is defined as [8]:

$$\Delta\chi = \frac{\lambda}{2\sin(\theta/2)} \quad (1)$$

where λ is the wave length of the laser beam and θ is the angle between the two laser beams, usually between 2 and 10^{o}. For an argon-ion laser beam of 0.514 μm wavelength, the typical fringe spacing would vary from 3 to 15 µm. A particle or an aerosol passing through the measuring volume scatters light from each of the two laser beams and causes a shift in frequencies, ν_D, which is given as [8]:

$$\nu_D = \frac{U}{\Delta\chi} = \frac{2U\sin(\theta/2)}{\lambda} \tag{2}$$

where U is the velocity of a particle passing through the measuring volume. The frequency shift is proportional to the particle (and fluid) velocity component perpendicular to the fringes, a standard arrangement in conventional PDAs.

When a particle or an aerosol crosses the measuring volume, it also scatters the laser beam in the form of a burst (also known as Doppler burst). These bursts are detected by two or more photomultipliers located at an optimal angle with respect to the plane of incident beams. The bursts of two laser beams from a particle reach the receiving optics at different time intervals or with a shift in phase. Figure 2 shows a typical set up where P1 and P2 are the photomultipliers arranged at a suitable off-axis angle φ (usually between 20 and 80^o) and symmetrically to the interference plane with equal elevation angle ψ (usually between 5 and 14^o) [9]. The relationship between the particle size and phase shift is given as follows [10]:

$$d = \frac{1}{2b}\left(\frac{\lambda}{\pi n_c}\right)\Delta\Phi \tag{3}$$

where d is the particle diameter, n_c is the refractive index of the medium, b is a function of the PDA optical arrangement (typical to a particular PDA set up), λ is the wave length of the laser beam and $\Delta\Phi$ is the phase shift between two receiving beams. Equation (3) shows that the particle diameter is proportional the phase shift between two receiving beams. The phase shift increases with increasing particle size. Since the phase has a 2π function, it cannot exceed 2π, i.e. 360°. A large particle can cause a phase shift greater than 2π, and a two-photomultiplier PDA cannot discriminate between this size and a much smaller particle. Therefore, a three-photomultiplier set-up is used in overcoming this ambiguity.

Figure 3 shows typical signals recorded by two photomultipliers as a particle crosses the measuring volume. Doppler bursts are recorded by each photomulitplier but with a phase shift between them. The recorded time difference, Δt, is related to the period, T, of a pair of Doppler bursts as follows [10]:

$$\Delta\Phi = \frac{2\pi(\Delta t)}{T} \tag{4}$$

Most commercial PDAs come with sophisticated computer software and other accessories for measuring various parameters of particles or aerosols in multi-phase flows. The software in the signal processor is an integral part of a PDA that evaluates the afore-mentioned correlations to measure velocity, droplet-size distribution, and in many cases, droplet concentration in a fluid flow of interest.

The PDA at AECL uses a variable power, water-cooled Argon-ion laser (wave length = 0.514 µm). A fiber optic probe fitted with a lens (focal length = 600 mm) forms the transmitting optics. The receiving optics consisted of a convex lens (focal length = 310 mm), and was placed at an off-axis angle of 65^o to receive the scattered light from the measuring volume. Three photomultiplier tubes were mounted on the receiving optics to obtain frequency and phase information from the

Doppler signals. A computer finally processed the signals and stored them as velocity and size distributions for individual test runs. The PDA was commissioned before starting the test series for uncertainty analyses of the measured parameters [11].

4. VELOCITY AND SIZE CALIBRATION

The PDA was calibrated for both size and velocity distributions, and the calibration was performed by conducting measurements in previously well-established flow fields (for velocity calibration) seeded with particles of a known size distribution (for size calibration).

The calibration for velocity was carried out using a TSI flow calibrator (Model 1125). Filtered air was used as the test fluid. The flow was artificially seeded with water particles (< 5 μm in diameter) generated by a custom-made aerosol generator. Water particles were introduced well ahead of the orifice mouth. Figure 4 shows an excellent agreement between the measured velocities and those calculated by using the pressure drop across the orifice.

Soda lime-glass beads of three known size distributions (manufacturer's specifications: Nominal diameter = 22.1±1.5 μm, 58.9±3.5 μm and 85.3±4.3 μm) were used as test particles for the droplet-size calibration. Each set of the glass beads was injected uniformly in an air medium flowing into the TSI flow calibrator well ahead of the orifice mouth. Figure 5 shows a relatively small span factor for each set of glass beads suggesting that these sets were measured within manufacturer's stated deviations.

5. FLASHING JET EXPERIMENTS

The flashing jet discharge from typical breaks in the PHTS was simulated with nozzles of different sizes that were characterized by the nozzle diameter, *D*, and the length-to-diameter (*L/D*) ratio. Figure 6 shows a schematic of the experimental set-up used in the study of flashing jets at AECL. The facility was instrumented with pressure transducers and thermocouples at strategic locations, and the data from these instruments were recorded by interfacing with a computer. The pressure vessel (pot boiler) was initially filled with water to about two-thirds height and boiled at atmospheric pressure for approximately 30 minutes to release any dissolved gas in the supply system. A vent atop the vessel was closed and the vessel was gradually pressurized with nitrogen gas added from the top. The water was heated to the required temperature by means of a heating source inside the vessel. After the test conditions (pressure and temperature) were attained, the pipe connecting the pressure vessel to the nozzle arrangement was heated to the required temperature. The pipe was also insulated to prevent any heat losses.

Flashing jet tests were performed using high-temperature (166 to 285^{o}C), high-pressure (1 to 10 MPa) subcooled water discharged through these nozzles. The nozzle assemblies consisted of simple round-hole nozzles, conical nozzles and nozzles fitted with extension pipes. Nozzle diameters varied from 0.61 to 2.4 mm, and the *L/D* varied from 0.5 to 200 depending on the nozzle type. The water initial temperature was maintained at about 8% below the saturation temperature corresponding to a selected initial pressure. For example, if the initial pressure was 10 MPa (saturation temperature = 311^{o}C), then the initial temperature was maintained at 285^{o}C (i.e., 8% below 311^{o}C) to ensure a stable jet (without any nucleation inside a nozzle). As the hot water depressurized through a nozzle, a flashing jet was formed, and the jet had the form of a rapidly expanding region followed by a linear spreading. Figure 7 shows that the initial expansion was ellipsoidal at lower pressures, whereas it became hemispherical at higher pressures.

5.1 Velocity Measurement

The jet velocity was measured at four axial stations (*Z/D* = 200, 400, 800 and 1600) with the help of the PDA. At each of these stations, measurements were also conducted along the horizontal direction (X-axis) and the vertical direction (Y-axis). The nozzle assembly was mounted on a traversing mechanism to facilitate movements in the axial direction (Z-axis) and the horizontal (X-axis) direction of the jet. Measurements along the vertical direction were achieved with simultaneously moving the transmitting and receiving optics of the PDA. In some cases, however, difficulties were encountered during measurements at axial location of *Z/D* = 200 for 7.5- and 10-MPa pressure tests. The main reason for this was the attenuation of the incident beam intensity due to large concentration of aerosols crossing the beam path, reduction in the scattered light intensity and possible presence of multiple aerosols in the measuring volume.

Figure 8 shows the axial velocity distribution measured along the centerline of the flashing jet for the 0.61-mm diameter nozzle. As expected, velocity decreased almost linearly with increasing distance from the nozzle exit. Higher initial water pressures produced higher jet velocities than those produced at lower pressures. Figure 9 shows the radial velocity distribution at two axial locations in flashing jet generated with test conditions of 4 MPa pressure and 230°C for the same nozzle. Velocities measured along the X- and Y-axes are normalized with the centerline velocity at the corresponding axial location. The radial locations were normalized using the half widths, δ, of the jet (radial location where the velocity was one half of the centerline velocity). All data seem to collapse onto a single normal distribution with the peak located at the center of the jet. For a qualitative comparison, the figure also shows a typical velocity distribution obtained in a single-phase flow [12].

5.2 Aerosol Size Measurement

The aerosol size distribution was measured along the axial direction as well as along the horizontal and vertical radial directions. A log-normal distribution is used extensively for aerosol size distributions because it fits the observed distributions reasonably well, and the distribution is generally characterized by the geometric mean diameter (GMD). The GMD is expressed as [13]:

$$GMD = \exp\left[\frac{\sum n_i \ln(d_i)}{N}\right] \tag{5}$$

where n_i is the number of aerosols in size interval i (in a size-count histogram) having a midpoint size d_i, and N is the total number of aerosols. Figure 10 shows the variation in GMD (usually expressed in μm in aerosol studies) along the jet axial locations as well as the effect of jet operating pressures. In general, the aerosol diameter decreased with increasing distance from the nozzle exit. The effect of jet operating pressure is evident only beyond *Z/D* longer than 800, i.e., the diameter usually increased with increasing pressure. The measured diameters along the horizontal (X-axis) direction were symmetrically distributed (Figure 11), however, they had an asymmetric vertical distribution with larger size aerosols crowding below the jet axis as shown in Figure 12. This asymmetry indicates that the larger aerosols had the tendency to gravitate along the lower half of the jet axis with the increasing Z/D.

6. CONCLUSIONS

A phase-Doppler anemometer is a non-intrusive optical device, and it was used successfully at AECL to measure aerosol size distribution and velocity in flashing water jets discharged from different nozzles simulating hypothetical breaks in the reactor heat-transport system operating at thermalhydraulic conditions of interest.

The axial jet velocity gradually decreased with increasing distance from the jet exit. The higher operating pressures produced higher jet velocities. Velocity measurements along the vertical and horizontal directions show symmetrical distributions.

Aerosol size decreased with increasing distance from the nozzle exit. Higher operating pressures produced larger aerosols. The gravitational settling affected the vertical size distribution that caused the larger aerosols to travel below the lower half of the jet axis. This effect was more predominant at axial locations further away from the nozzle exit.

ACKNOWLEDGEMENT

The author would like to thank R. Balachandar, M. Hogeveen-Ungurian and S.R. Mulpuru for performing the tests, and acknowledge the funding provided by AECL and the CANDU Owners Group (COG).

REFERENCES

[1] M. Razzaghi, Droplet size estimation of two-phase flashing jets, *Nuclear Eng. Design,* 114, 115-124, 1989.
[2] An internal publication of the Atomic Energy of Canada Ltd. (AECL).
[3] H.W.M. Witlox and P.J. Bowen, Flashing liquid jet and two-phase dispersion (a review), *Health and Safety Executive (HSE) Contract Research Report 403*, 2002, St. Clements House, 2-16, Colegate, Norwich, UK.
[4] R. Brown and J.L. York, Sprays formed by flashing jets, *A.I.Ch.E. Journal*, 8(2), 149-153, 1962.
[5] H.H. Qui and M. Sommerfeld, A reliable method for determining the measurement volume size and particle mass fluxes using phase-Doppler anemometry, *Expt.Fluids*, 13, 393-404, 1992.
[6] M. Sommerfeld and H.H. Qui, Particle concentration measurements by phase-Doppler anemometry in complex dispersed two-phase flow, *Expt. Fluids*, 18, 187-98, 1995.
[7] W.D. Bachalo, R.C. Ridoff and A.B. de la Rosa, Mass flux measurements of a high number density spray system using the phase-Doppler particle analyzer, *AIAA 26th Aerospace Science Meeting*, Reno, Nevada, January 11-14, 1988.
[8] F. Durst, A. Melling and J.H. Whitelaw, Principles and Practice of Laser-Doppler Anemometry, Academic Press, London, 1976.
[9] Aizu, J. Domnick, F. Durst, G. Grehan, F. Onofri, H.H. Qui, M. Sommerfeld, T.H. Xu and M. Ziema, New generation of phase-Doppler instruments for particle velocity, size and concentration measurements, *Particle & Particle Systems Characterization*, 11, 43-54, 1994.
[10] U. Manasse, T. Wriedt and K. Bauckhage, Phase-Doppler sizing of optically absorbent single- and multi-component liquid droplets using semiconductor devices, *Meas. Sci. Technol.,* 4, 369-377, 1993.
[11] S.R. Mulpuru, R. Balachandar and M.H. Ungurian, Phase-Doppler anemometer commissioning tests for measurement of water aerosol sizes and velocities in flashing jets, *Nuclear Eng. Design*, 166, 443-452, 1996.
[12] G. Hetsroni and M. Sokilov, Distribution of mass, velocity and intensity of turbulence in a two-phase turbulent jet, *J. Appl. Mech.*, 315-327, 1971.
[13] W.C. Hinds, Aerosol Technology, John Wiley & Sons, New York, 1982.

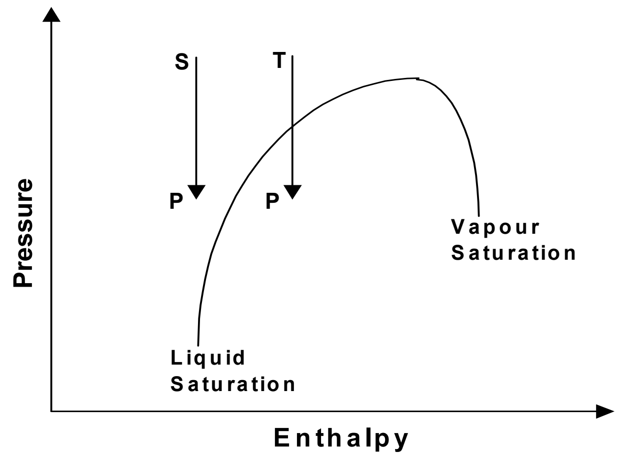

Figure 1: Thermodynamic representation of a flashing jet

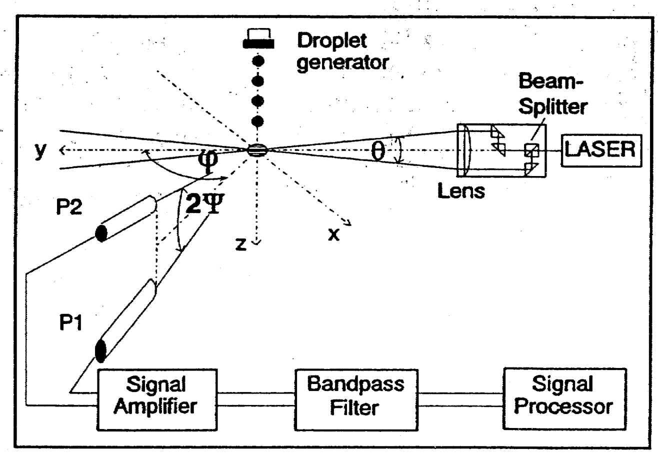

Figure 2: Schematic of a phase-Doppler anemometer [10]

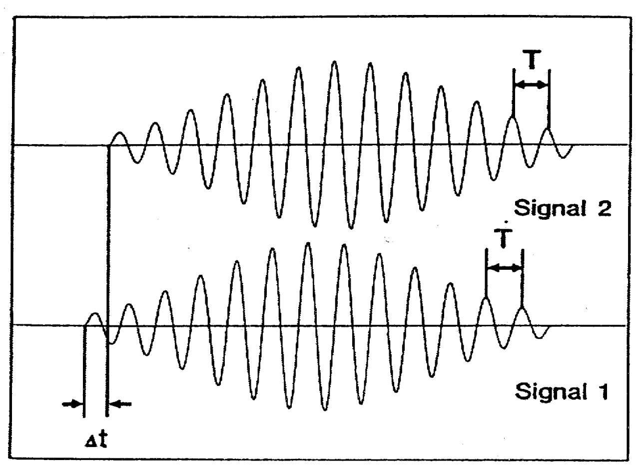

Figure 3: Phase difference between two Doppler bursts [10]

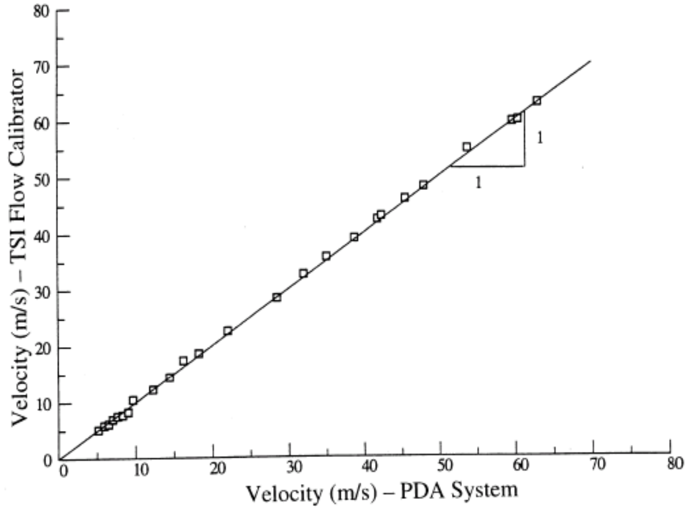

Figure 4: Phase-Doppler anemometer velocity measurement validation

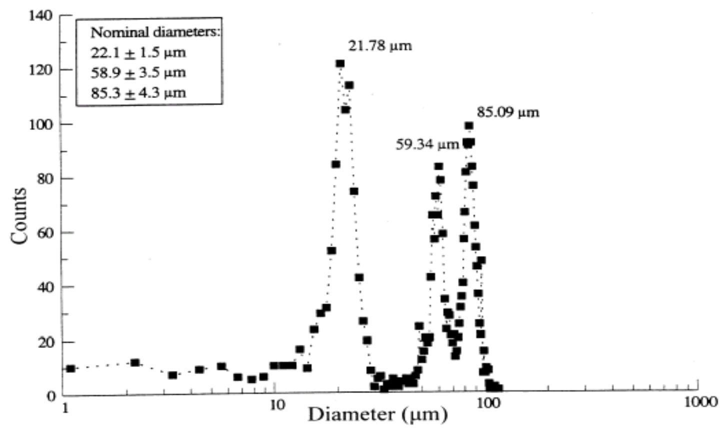

Figure 5: Count-size histogram of a mixture of glass beads for size validation

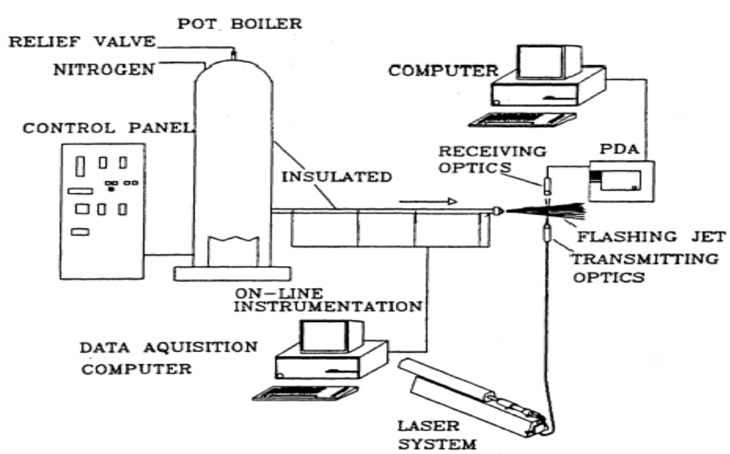

Figure 6: Schematic of the experimental set-up

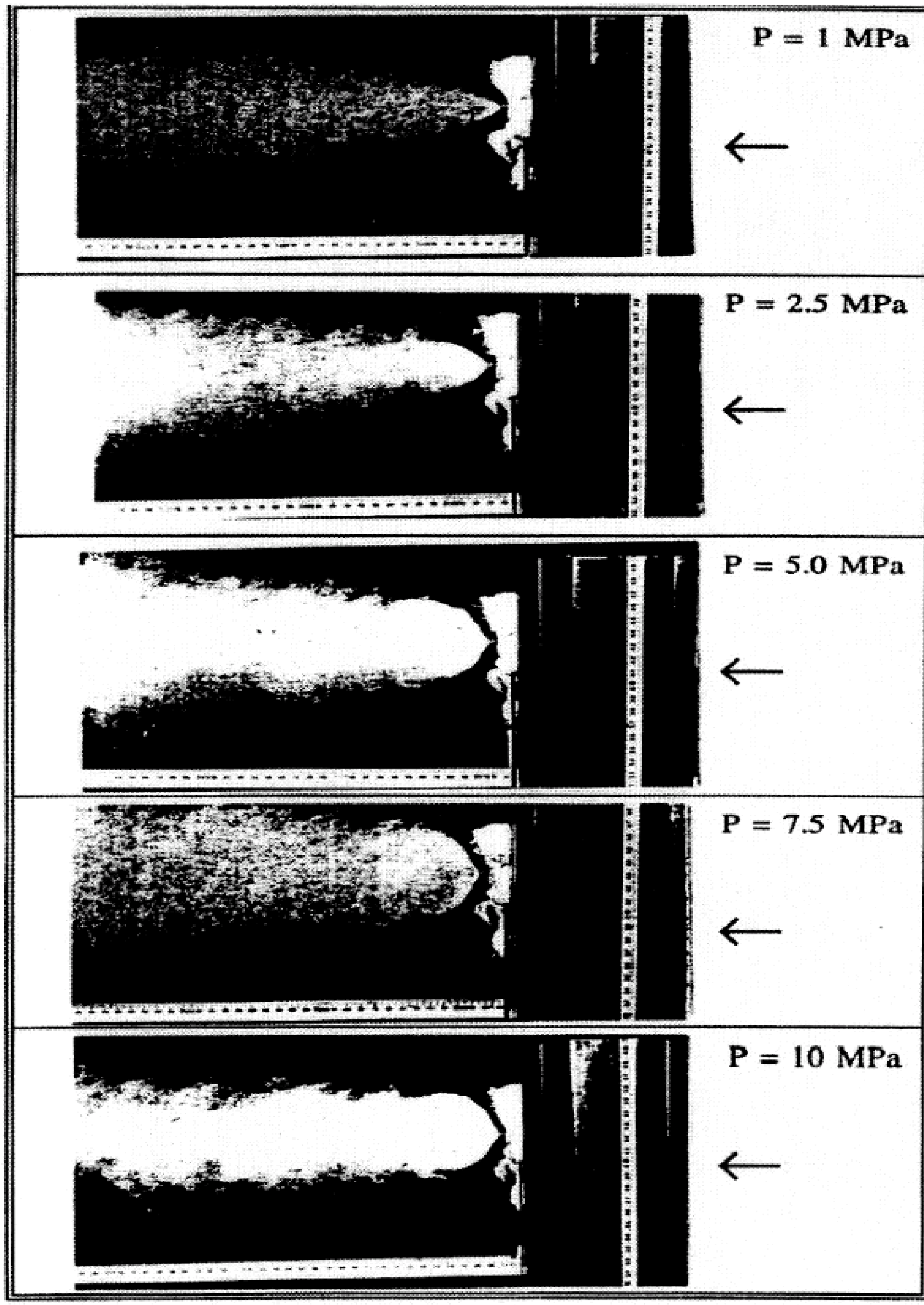

Figure 7: Jet shape at different inlet pressures for the 0.61-mm diameter nozzle

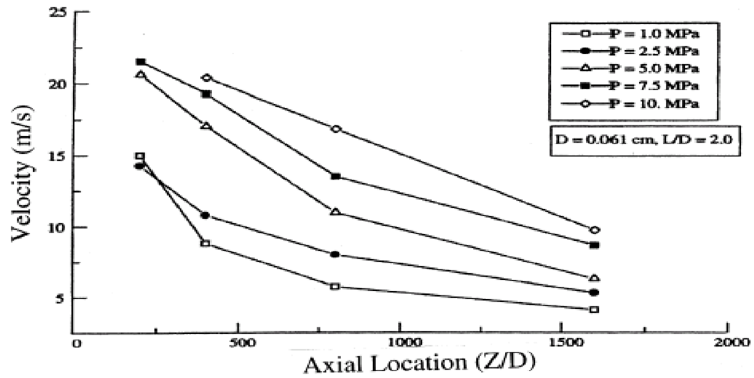

Figure 8: Jet axial velocity as a function of pressure

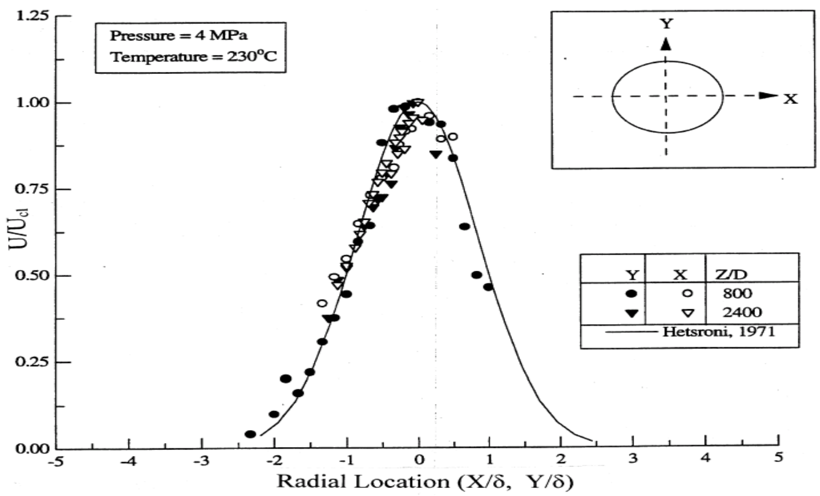

Figure 9: Radial distribution of velocity at various axial locations

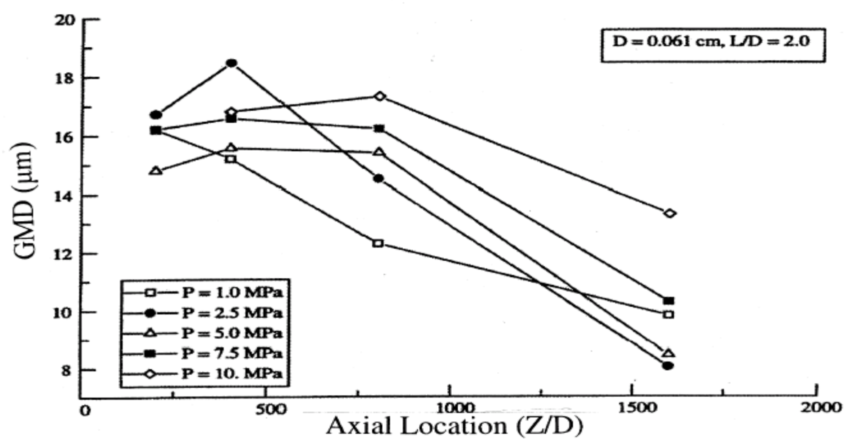

Figure 10: Geometric mean diameter of aerosols as a function of pressure

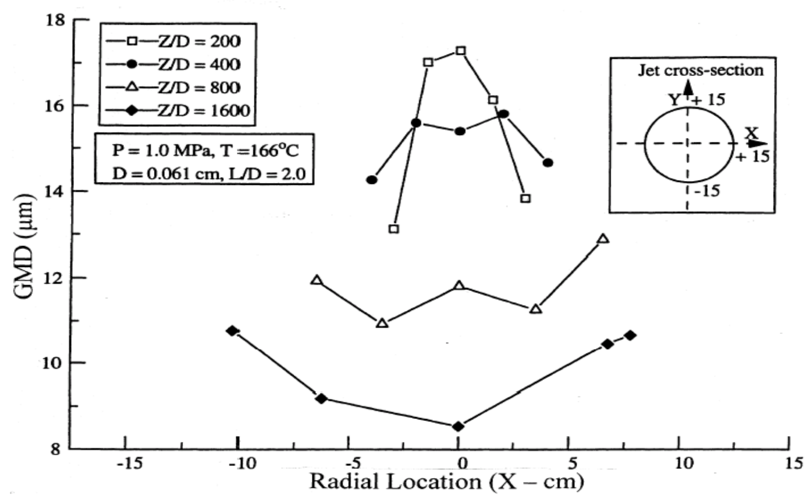

Figure 11: Aerosol size distribution at different radial (X-axis) locations

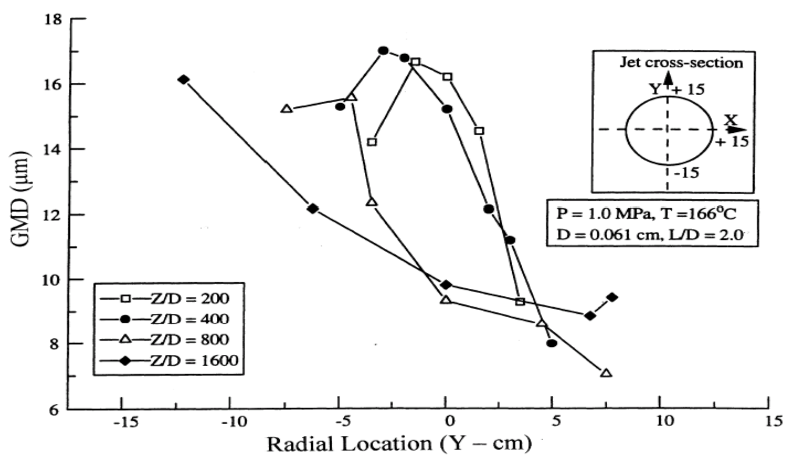

Figure 12: Aerosol size distribution at different vertical (Y-axis) locations